POTSDAM-INSTITUT FÜR
KLIMAFOLGENFORSCHUNG

EPJ manuscript No.
(will be inserted by the editor)

Local vs global redundancy – trade-offs between resilience against cascading failures and frequency stability

Anton Plietzsch[1,2,a], Paul Schultz[1,2,b], Jobst Heitzig[2,c], and Jürgen Kurths[1,2,3,4]

[1] Institute of Physics, Humboldt University of Berlin, 12489 Berlin, Germany
[2] Potsdam Institute for Climate Impact Research, 14412 Potsdam, Germany
[3] Institute for Complex Systems and Mathematical Biology, University of Aberdeen, Aberdeen-AB243FX, United Kingdom
[4] Department of Control Theory, Nizhny Novgorod State University, 606950 Nizhny Novgorod, Russia

Abstract. When designing or extending electricity grids, both frequency stability and resilience against cascading failures have to be considered amongst other aspects of energy security and economics such as construction costs due to total line length. Here, we compare an improved simulation model for cascading failures with state-of-the-art simulation models for short-term grid dynamics. Random ensembles of realistic power grid topologies are generated using a recent model that allows for a tuning of global vs local redundancy. The former can be measured by the algebraic connectivity of the network, whereas the latter can be measured by the networks transitivity. We show that, while frequency stability of an electricity grid benefits from a global form of redundancy, resilience against cascading failures rather requires a more local form of redundancy and further analyse the corresponding trade-off.

Key words. power grid – blackout – cascading failures – basin stability – transitivity – random network

Contents

[a] e-mail: antonp@physik.hu-berlin.de
[b] e-mail: pschultz@pik-potsdam.de
[c] e-mail: heitzig@pik-potsdam.de

1 Introduction

The transformation of the electrical energy supply from large, centralised power plants based on nuclear or fossil fuels to smaller, decentralised sources based on renewable energies not only poses an enormous challenge for the design and stable operation of the grid, but points to the crucial influence the weather and hence also climate change has on the power grid. At the same time, the complex topology of interconnections in the power grid makes it hard to foresee the consequences of single-element disturbances or failures. The following two rather recent events illustrate the necessity of an systemic assessment of electrical power supply networks.

In November 2006 a large blackout occurred in the continental European power grid, leading to power supply disruptions for more than 15 million households. On this particular day, there were significant East-West power flows as a result of international power trading and an unusually large feed-in of wind power in North-West Germany. After a manual disconnection of the 380 kV power line Conneforde-Diele for the transit of the ship "Norwegian Pearl" via the Ems River to the North Sea, the resulting physical power flow on the 380 kV Landesbergen-Wehrendorf line was very close to the secure limit. Hence, a relatively small power flow fluctuation was able to trigger a cascade of failure in several high-voltage lines. This split the European grid into three separate components (West, North-East and South-East) with significant power imbalances in each area. The power imbalance in the Western part in particular induced a severe frequency drop that caused an interruption of supply in several European countries [33].

In July 2012 two severe blackouts affected the power grid in north and east India, leaving more than 620 million people without electricity at certain times. The power system of this country is divided into five regional grids (Northern, Western, Southern, Eastern and North-Eastern) which are all interconnected. On both occasions, the grid disturbance was initiated by tripping of the 400 kV Bina-Gwalior power line, separating the Northern region from the rest of the grid. Already prior to the failure of this line the grid was operating under difficult conditions due to a large number of line outages. Effectively, the 400 kV Bina-Gwalior-Agra line was the only main AC circuit available between the Western and the high-demand Northern regions. The power deficit was worsened by a late arrival of the summer monsoon which lowered hydroelectric power generation and increased the energy demand for air conditioning because of high temperatures. The first grid disturbance led to a collapse of the Northern region's grid due to a critically low local grid frequency. The day after, while the grid recovered from the prior black out, another major disturbance took place. This time the cascaded line tripping caused a near-total blackout in the Northern, North Eastern and Eastern systems [8].

These two examples reveal how a high share of variable renewable energy resources in the power generation mix may, in combination with certain natural or purely man-made extreme events (extreme weather conditions vis-à-vis intentional

line interuptions), lower the resilience of the power supply. Under such critical conditions, the failure of a single power line can cause large *cascading failures* with grid blackouts as a consequence. Since electric power transmission systems are a key infrastructure, such blackouts have major consequences for the economy and national security. At the same time, power outages affect medical services, emergency response and public health efforts. Moreover, case studies indicate that large outages can have significantly more severe consequences on public health than an equally sized combination of smaller ones, due to several complex interactions and feedbacks with other infrastructure networks [2,13,19,24]. Considering the worldwide growth of renewable energy capacity [26] as well as the increasing impact and frequency of extreme weather events due to climate change [18], the stable operation of power grids will stay a major challenge over the next decades. It is therefore an important task to study the stability and resilience of power grids [5,12,32] in order to better address the threat of large-scale blackouts in the future.

The aim of this article is to study in the framework of complex network theory how the topological design of a power grid influences its resilience against cascades of power line trippings like those described above and compare it to the grid's frequency stability. Power grids can be described as complex networks with nodes representing generators and consumers, and links representing transmission lines [7,10,25,27]. Although there has been a lot of research on network dynamics of cascading failures (for instance [4,17,23]) in general complex networks without specific assumptions about their internal dynamics, only few approaches are suitable to describe the dynamics of cascading failures of transmission lines observed in real power grids [3,31].

In Sec. 2, we generalise the model of [3] by replacing its small-angle linearisation by more detailed nonlinear equations for the alternating current power flow, which we then apply in Sec. 3 to ensembles of synthetic power grid topologies generated with the model of [29] to study the influence of the grid topology on resilience against cascading failures. We find that one of the most influential topological characteristics is *local redundancy* as measured by the network's *transitivity*. This can be explained by the requirement to reroute the power originally flowing through a tripped line along a detour and the fact that the longer the detour, the more likely the increased flow along it will cause another tripping. Since a high transitivity implies the existence of many very short (length two) detours, it hence decreases the probability that an initial tripping develops into a cascade.

In Sec. 4, we compare this finding to the influence of redundancy on another important aspect of energy security, *frequency stability* even under large perturbations, for which we use the recently introduced non-linear measure of basin stability [21,22]. In contrast to cascading failures, we find that the grid's overall frequency stability does not benefit from local but rather from *global redundancy* as measured by the network's *algebraic connectivity*, although the individual frequency stability of certain nodes in detours also profits from local redundancy [30]. Since the total length of all lines of the grid is typically limited due to economic and/or political restrictions, this poses a trade-off problem between local and global redundancy that we summarise in a trade-off diagram. Sec. 5 concludes with a recommendation for a heuristic rule-of-thumb for placing additional grid lines and suggestions for future research.

2 Modelling cascading failures

As in any complex real-world system, failures and disruptions cannot be fully avoided when operating power grids. If an element of the power system is damaged it has to be disconnected immediately from the rest of the system in order to avoid further damage to, or disturbance of, neighboring elements. The detection of a problem and

subsequent disconnection of the faulty element is usually done automatically by protective relays and circuit-breakers, which operate according to a variety of physical principles [20].

The most common failures of transmission lines are due to short circuits: although overhead transmission lines are shielded from lightning by grounded wires, lightning strikes remain the most common cause of line failure. The majority of these problems are temporary and are mostly caused by flashovers. Lines which are affected can then usually be reconnected to the system after a short time. However, in the case of permanent damage the line is immediately tripped again by the protection system [20].

In most cases, the rest of the power system is not affected by failures of single transmission lines. Nevertheless, under certain extreme conditions like those described in the introductory examples, the failure of a line can cause further failures. A large amount of blackouts in power grids is caused by such cascades of line tripping. If a generator or consumer is disconnected from the rest of the grid, the disconnection causes a power imbalance in the system. This imbalance is immediately compensated by a deceleration or acceleration of the generators, which causes changes in frequency. Thus, in order to stabilise the system's frequency within the narrow limits desired for other stability reasons, there has to be a frequency control mechanism. When the change in power demand is slow, this is done by switching some generating units on or off for half-hour intervals. If there are faster changes of frequency, however, there has to be a faster, automatic control of the generators. As a first step, some power generation is immediately increased or decreased proportional to the frequency deviation in the so-called primary control. There are also secondary and tertiary control mechanisms taking place over longer time scales [20]. This complex reorganisation of the system in order to alleviate effects of a perturbation can be considered a prime example of a complex system's *resilience* in the sense of Holling [16] (see also [11]).

In the case of a cascading failure blackout, large parts of the power grid can become disconnected simultaneously. Usually, this is caused by large power imbalances within those parts leading to a drop of frequency that is too large to be offset by the primary control.

2.1 Existing models

A model for cascades of overload failures in a network was introduced by Motter and Lai [23] in 2002. They assumed that in a given network one unit of the relevant quantity is exchanged along the shortest path between every pair of nodes in the network at each time step. Therefore, the load of a node j can be measured by its shortest-path betweenness b_j. The capacity of a node j is the maximum load it can handle and is defined as

$$C_j = (1 + a) \cdot b_j(t_0), \tag{1}$$

where $b_j(t_0)$ is the initial betweenness and $a \geq 0$ is a tolerance parameter. When a node i is removed from the network, the betweenness of node j may change. If the load thus becomes larger than the capacity, the node j fails and is also removed from the network. This process of redistribution of loads and node removals can then lead to a cascade of failures. The damage caused by such a cascade is quantified in terms of the relative size f_{LC} of the largest component remaining. The first node to be removed, triggering the cascade, is either the one with the highest initial load or selected randomly from the network. For both cases the authors demonstrated that the removal of only one key node can trigger a large-scale cascade causing the entire network to collapse. However, this model is not suitable for modelling cascading failure blackouts in power grids. On the one hand, it is a model for node failures whereas in

power grids the failing devices are usually the lines. Moreover, for power flows it is a wrong assumption that quantities are only exchanged along the shortest paths and therefore, the shortest-path betweenness is no appropriate measure for the load.

A more realistic model for cascading failures in power grids was proposed by Carreras et al. [3]. In this model each node is characterised by its input power P_i which is positive for generators and negative for consumers. The generator power is limited as $0 \leq P_i \leq P_i^{\max}$ and the consumer power as $P_i \leq 0$. For any given power demand the combination of generator powers is found via cost-optimisation. The resulting distribution of input power values leads to power flows F_{ij} on the links. Each of those links is characterised by the impedance Z_{ij} and the maximum power flow $F_{ij}^{\max}$ it can carry. The power flows F_{ij} are then calculated using the DC power flow equations. In fact, the DC power flow model presented here is a linearisation of an AC power flow model (cf. Sec. 2.2) with the approximation $\sin(\theta) \approx \theta$ for the voltage angles θ. If the power flow exceeds the link capacity, as defined by

$$C_{ij} = (1 - b) \cdot F_{ij}^{\max}, \tag{2}$$

with a tolerance parameter b, the link fails and the power flow is redistributed. This model was tested on idealised tree networks and the IEEE 118-bus network. The authors identified two critical points that result from the limits of the links and generators. Close to these critical points the model shows similar characteristics as real blackout data.

2.2 AC power flow equations

Power-flow studies are an important engineering tool for the design of future power systems as well as determining the best operational parameters for existing systems. The AC power flow equations give the relations between the magnitude and phase angle of the voltage at each node, and the real and reactive power flows in each line. For realistic power grids, this system of nonlinear equations can only be solved numerically [14].

The power grid network consists of N nodes connected via transmission lines.. Every line j–k connecting two nodes in the grid is characterised by its impedance $z_{jk} = r_{jk} + ix_{ij}$, where r_{jk} is the resistance and x_{jk} the reactance. The inverse of the impedance is called admittance $y_{jk} = z_{jk}^{-1}$, a complex variable that can be written as $y_{jk} = g_{jk} + ib_{jk}$ with the conductance g_{jk} and the susceptance b_{jk}. It is useful to define a nodal admittance matrix Y as

$$Y_{jk} = G_{jk} + iB_{jk} = \begin{cases} \sum_l a_{jl} y_{jl} & \text{for } j = k \\ -y_{jk} & \text{for } a_{jk} = 1 \\ 0 & \text{otherwise,} \end{cases} \tag{3}$$

where G and B are the nodal conductance and susceptance matrices and $A = (a_{jk})$ is the adjacency matrix. The matrix Y is a generalisation of the Laplacian matrix L with the line admittances y_{jk} as weights. Using this, the net current injected at node j can be written as follows:

$$\begin{aligned} I_j &= \sum_k a_{jk} y_{jk} (V_j - V_k) = V_j \sum_k a_{jk} y_{jk} - \sum_k a_{jk} V_k y_{jk} \\ &= V_j Y_{jj} - \sum_k a_{jk} V_k y_{jk} = \sum_k (\delta_{jk} Y_{jk} - a_{jk} y_{jk}) V_k \\ &= \sum_k Y_{jk} V_k. \end{aligned} \tag{4}$$

The complex voltage at node j is given in polar coordinates by

$$V_j = |V_j|(\cos\theta_j + i\sin\theta_j). \tag{5}$$

As a consequence, the complex power can be written as

$$P_j + i\cdot Q_j = V_j \cdot I_j^* = V_j \sum_k Y_{jk}^* V_k^* = |V_j| \sum_k |V_k|(G_{jk} - iB_{jk})e^{i\theta_{jk}}, \tag{6}$$

with the real and reactive powers

$$P_j = |V_j| \sum_k |V_k|(G_{jk}\cos\theta_{jk} + B_{jk}\sin\theta_{jk}), \tag{7}$$

$$Q_j = |V_j| \sum_k |V_k|(G_{jk}\sin\theta_{jk} - B_{jk}\cos\theta_{jk}), \tag{8}$$

and the voltage angle differences $\theta_{jk} = \theta_j - \theta_k$. In this study only real power will be considered. For high-voltage transmission lines, the line resistances can be neglected ($r_{jk} \approx 0$) and the expression for real power simplifies to

$$P_j = \sum_k a_{jk} \frac{|V_j||V_k|}{x_{jk}} \sin\theta_{jk}. \tag{9}$$

The reactance is approximately proportional to the spatial line length, hence approximately equal to $x_{jk} = x' \cdot d(j,k)$, where $d(j,k)$ is the Euclidean distance and x' the specific reactance per length [20]. If all input powers P_j and voltages V_j at the nodes as well as the line reactances are given, the nonlinear system of equations (Eqn. 9) is then solved numerically in order to get the stationary voltage angle differences $\tilde{\theta}_{jk}$. With these, the power flow in the transmission lines is

$$F_{jk} = \frac{|V_j||V_k|}{x_{jk}} \sin\tilde{\theta}_{jk}. \tag{10}$$

Generally, we will assume that $|V_j| = |V_k| = 380$ kV. The specific reactance is chosen to $x' = 0.265\ \Omega/\text{km}$ [20] such that the average reactance corresponds to a 200 km transmission line, where the line length distribution is controlled by the network model described in Sec. 3.1.

2.3 Improved model of cascading failures

We can now construct an improved model based on actual power flow calculations instead of topological network measures. In addition to the dynamics of line trippings, it contains an algorithm modelling the power regulation at the node level. The model has some similarities with the one proposed by [3], but it differs in a few important assumptions. In the model proposed here, the AC power flow equations are not linearised in the small-angle approximation. Second, all initial input powers have the same absolute value and are distributed randomly over the network instead of following cost-optimisation processes (Fig. 2). The latter assumption may be less realistic, but it allows generating a variety of scenarios with different power flow dynamics for one single network topology. Finally, we assume that for each such scenario lines are built with a flow capacity that only depends on a global tolerance parameter and the expected power flow on that specific link in the undisturbed network state.

2.3.1 Initialisation

Every node of the graph is either a power consumer or a power generator and every link is a transmission line. We assume that exactly one half of the nodes are consumers having a negative power input and the other half are generators with positive power input. The assignment of nodes to one of these groups is random. In the beginning, the absolute value of power input of all nodes are equal $|P_0| = 1$. The reactance of all links is $x_{ij} = x' \cdot d(i,j)$, where $d(i,j)$ is the Euclidean distance and x' the specific reactance per length.

With the given network topology and power inputs, the power flow F_{ij} can be calculated using the AC power flow model in Sec. 2.2. The secure limit for the power flow is given by the capacity

$$C_{ij} = (1+a)F_{ij}(t_0) \tag{11}$$

with the *tolerance parameter* a and the initial power flow $F_{ij}(t_0)$. Finally, a single link is randomly chosen and removed from the network. The resulting redistribution of power flow may lead to overloads in other links and hereby trigger a cascading failure.

2.3.2 Power Regulation

When a cascading failure of links occurs, the network might become disconnected into isolated components. Since the sum of all power inputs into every single component of the network has to be zero, the power input at every node is regulated using the following equation:

$$P_i' = P_i - \frac{1}{N(\mathcal{C})} \sum_{j \in \mathcal{C}} P_j, \tag{12}$$

where $N(\mathcal{C})$ is the number of nodes in the component $\mathcal{C}$. In other words, we assume that excess supply or demand is compensated equally by all nodes in a component. If a node is disconnected from the rest of the grid it becomes inactive, i.e. the power input is set to zero (Eqn. 12). The same applies to components with only one kind of nodes, either generators or consumers. In order to keep the algorithm as simple as possible without making further assumptions about the generators or consumers, we assume an ideal controllability of the nodes, i.e. P_i is not constrained and can be varied instantly in every time step.

2.3.3 Cascading Failure

The model for cascading failures of links is based on an iterative solution of the AC power flow equations (Eqn. 9, 10) and the removal of overloaded links in each time step. The flow capacity of a link is given by (Eqn. 11). Hence, the algorithm for the propagation of a cascading failure after the initial removal of a randomly chosen link is as follows:

1. Regulate the power input in every component of the network with (Eqn. 12).
2. Calculate the power flow F_{ij}.
3. If $F_{ij} > C_{ij}$, remove link from the network.
4. Repeat steps 1–3 until no more links are removed in step 3.

The damage caused by a cascade is then quantified in terms of the relative size f_{LC} of the largest component remaining. A step by step visualisation of single cascading failure process is shown in Fig. 1.

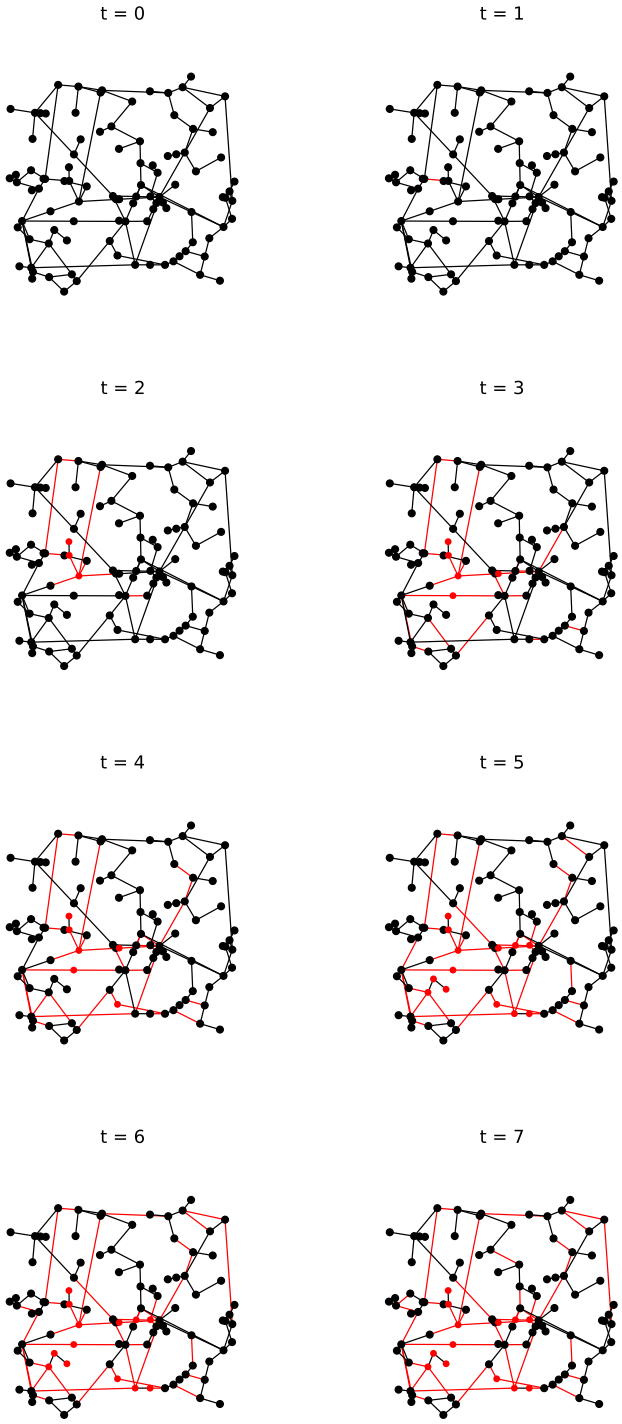

Fig. 1: Time steps of a cascading failure. The model's tolerance parameter was set to $a = 0.5$. The network is a random power grid generated by the model [29] with the parameters $\{N, N_0, p, q, r, s\} = \{100, 1, 0.3, 0.1, 1, 0.2\}$. Failed links and inactive nodes ($P = 0$) are colored red.

3 Influence of grid topology on cascading failures: local redundancy

For real-world applications, the influence of network topology on cascading failures is very important since improving it in an intelligent way may sometimes be cheaper than simply adding capacity on existing lines. Since the exact topological data of real world power grids is mostly unavailable or confidential, the simplest approach is to model them with randomly generated networks. However, most of these models are not appropriately reproducing the topological properties of real power grids. A network model which was designed to reproduce these properties was proposed recently [29] and is therefore used here.

3.1 Generating synthetic ensembles of realistic power grid topologies

The model of [29] is a random growth model with the topological properties of real power grids and other spatially embedded infrastructure networks. It uses the following heuristic redundancy/cost optimisation function when adding links:

$$f_r(i,j) = \frac{(d_G(i,j)+1)^r}{d(i,j)}, \tag{13}$$

where $d_G(i,j)$ is the length of a shortest path (i.e. the minimal number of traversed links) between nodes i,j in network G, $d(i,j)$ is the spatial Euclidean distance and $r \geq 0$ is a *redundancy trade-off parameter*. The network construction consists of an initialisation and a growth phase. The network is initialised at some size $N_0 > 0$ as follows, where $p, q \in [0,1]$ are two further parameters of the model:

1. Distribute N_0 nodes at random positions.
2. Initialise a minimum spanning tree using the spatial distance $d(i,j)$.
3. Set $m = N_0(1-s)(p+q)$. For $a = 1...m$ add a link between those two unlinked nodes for which $f_r(i,j)$ is maximal.

Then the network is extended node by node up to some size $N \geq N_0$ as follows, using another model parameter $s \in [0,1]$. For each new node $i = N_0 + 1 \dots N$, either perform step 5 (with probability s) or steps 1-4 (with probability $1-s$), where s is another parameter of the model:

1. Set a node i at a random position.
2. Find the node j for which $d(i,j)$ is minimal and add the link $i-j$.
3. Find another node k for which $f_r(i,k)$ is maximal and add the link $i-k$ with probability p.
4. Select an existing node i' at random, find the node k' for which $f_r(i',k')$ is maximal, and add the link $i'-k'$ with probability q.
5. Remove an existing link $a-b$ at random, set a node at the position $x_i = (x_a+x_b)/2$ and add the links $a-i$ and $i-b$.

3.2 Choice of parameters

In [29], the parameters $p, q, s \in [0,1]$ have been roughly estimated by fitting the model to data on real-world power grids, resulting in $p = 0.3, q = 0.1, s = 0.2$, see Fig. 2. Due to the computational effort we use relatively small networks of $N = 100$ nodes. An example for such small and isolated networks are power grids on islands [9]. Because a reliable estimate of N_0 would require historical data, we choose to put $N_0 = 1$ here,

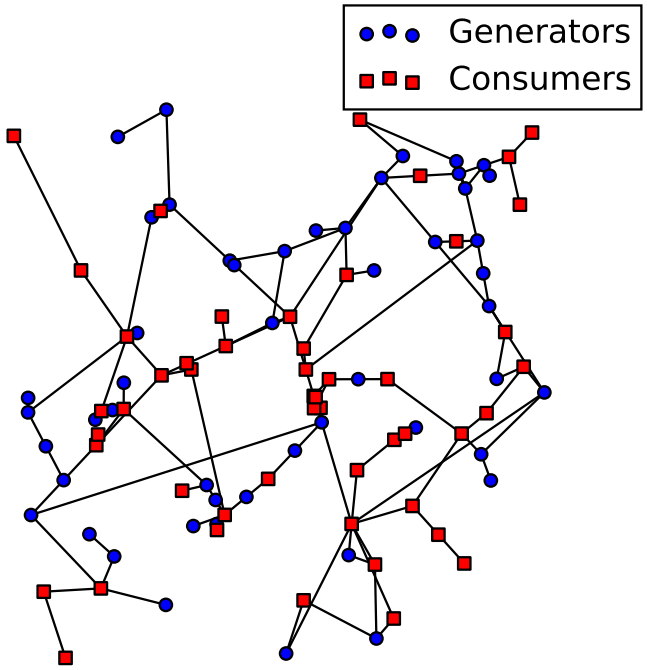

Fig. 2: Network generated with the random power grid model. The parameters used are $\{N, N_0, p, q, r, s\} = \{100, 1, 0.3, 0.1, 1, 0.2\}$.

which should not have a significant impact on the dependency on r, since r is used in the initialisation and growth phases in equivalent ways. Since our focus here is on the influence of redundancy, which is mainly governed by the parameter r, we use the above fixed values of p, q, s, a typical network size of $N = 100$ and vary r. Random power grids with small values of r minimise the line length and are hence extremely localised, increasing the probability for the existence of triangles (see Fig. 3a), that is, of local redundancy. A good standard measure of local redundancy is the *transitivity*, defined as the relative fraction of 3-loops in the network

$$T = \frac{\sum_{i,j,k} a_{ij} a_{jk} a_{ki}}{\sum_{\substack{i,j,k \\ i \neq j}} a_{jk} a_{ki}}, \tag{14}$$

where $A = (a_{ij})$ is the adjacency matrix. Transitivity is a global measure for clustering in a network, however it is different from the average local clustering coefficient. We

avoid using the term global clustering coefficient which has been used inconsistently for both definitions.

In contrast, in random power graphs with large values of r, global redundancy is maximised instead, i.e., distant nodes are interconnected more frequently. A good standard measure of global redundancy is the *algebraic connectivity* λ_2, defined as the second-smallest eigenvalue of the Laplacian matrix of the network.

As a consequence, the probability for the occurrence of triangles decreases (see Fig. 3b) when the total number of links, which is governed by the parameters p, q, is kept constant.

The local and global redundancies of random power grids with different r, as measured by the transitivity and the algebraic connectivity, are given in Fig. 5. The main region of r in which T and λ_2 vary considerably is the interval $[0.01, 10]$, hence we vary r over this interval.

For the underlying rationale and exact meaning of the other parameters p, q, s, we refer to [29].

Since loads between 50% and 70% seem to be realistic values for power flows on transmission lines [1], we choose the global excess capacity parameter of the links to $a = 0.5$.

3.3 Results from Monte-Carlo simulations

As explained above, redundancy is an important property to ensure the stability of power grids. In order to study this property, the tuning parameter r in the cost/redundancy optimisation function (Eqn. 13) was varied. For $r = 0$ the function minimises the total spatial length of links in the network, which leads to local redundancy, whereas for $r \to \infty$ the amount of global redundancy is maximised.

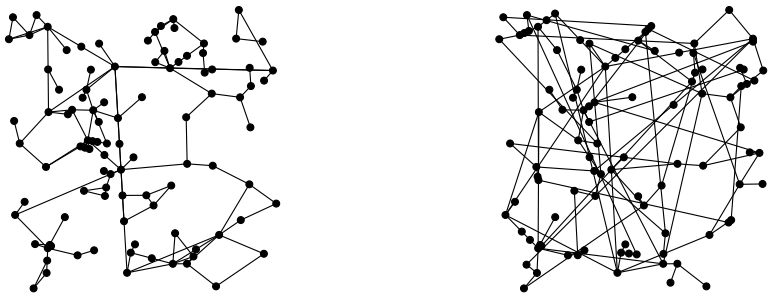

(a) $r = 0$ **(b)** $r = 10$

Fig. 3: Random power grids with different cost/redundancy optimisations. The varied parameter r is the tuning parameter in the cost/redundancy optimisation function (Eqn. 13). The other parameters of the network model are $\{N, N_0, p, q, s\} = \{100, 1, 0.3, 0.1, 0.2\}$.

For every value of r in the interval $[0.01, 10]$ we generated ensembles of 100 different network realisations with $N = 100$ nodes using following the set of parameters $\{N_0, p, q, s\} = \{1, 0.3, 0.1, 0.2\}$. The global excess capacity parameter was set to $a = 0.5$, thus the load of of every link is approximately 67% in the unperturbed state. For each value of r, cascading failures were triggered for 100 randomly chosen initial line removals each on 100 different initial network topologies. The damage was measured in terms of the relative size f_{LC} of the largest component remaining. The result is given in Fig. 4.

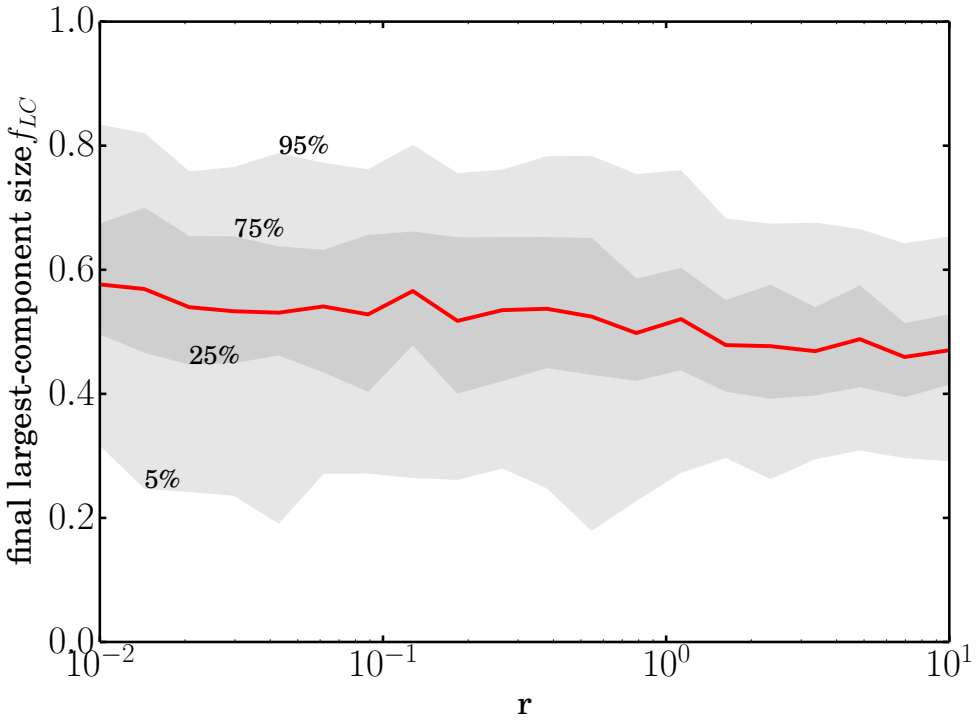

Fig. 4: Size of largest remaining component after cascading failures in random power grids with different cost/redundancy optimisations. The varied parameter r is the tuning parameter in the cost/redundancy optimisation function (Eqn. 13). The solid red line gives the mean value and the shaded regions correspond to the 5-th, 25-th, 75-th and 95-th percentiles of the distribution for each r-value. A linear regression of the mean gives a negative slope of -0.033 (p-value $= 1.1 \cdot 10^{-7}$).

Perhaps surprisingly, networks are more affected by cascading failures as r increases, i.e. networks with a more global redundant topology are more vulnerable. The average number of remaining connected nodes decreases by ca. 20% when r is increased in the considered parameter range. Thus, global redundancy is clearly not the only topological property that determines the resilience of a network. Looking at Fig. 5 reveals why: as the global redundancy as measured by the algebraic connectivity increases with increasing r, the local redundancy as measured by the transitivity decreases drastically, resulting in significantly fewer short detours around tripping lines and hence a higher probability that another line will trip and the grid will separate into more components, lowering the size of the largest component.

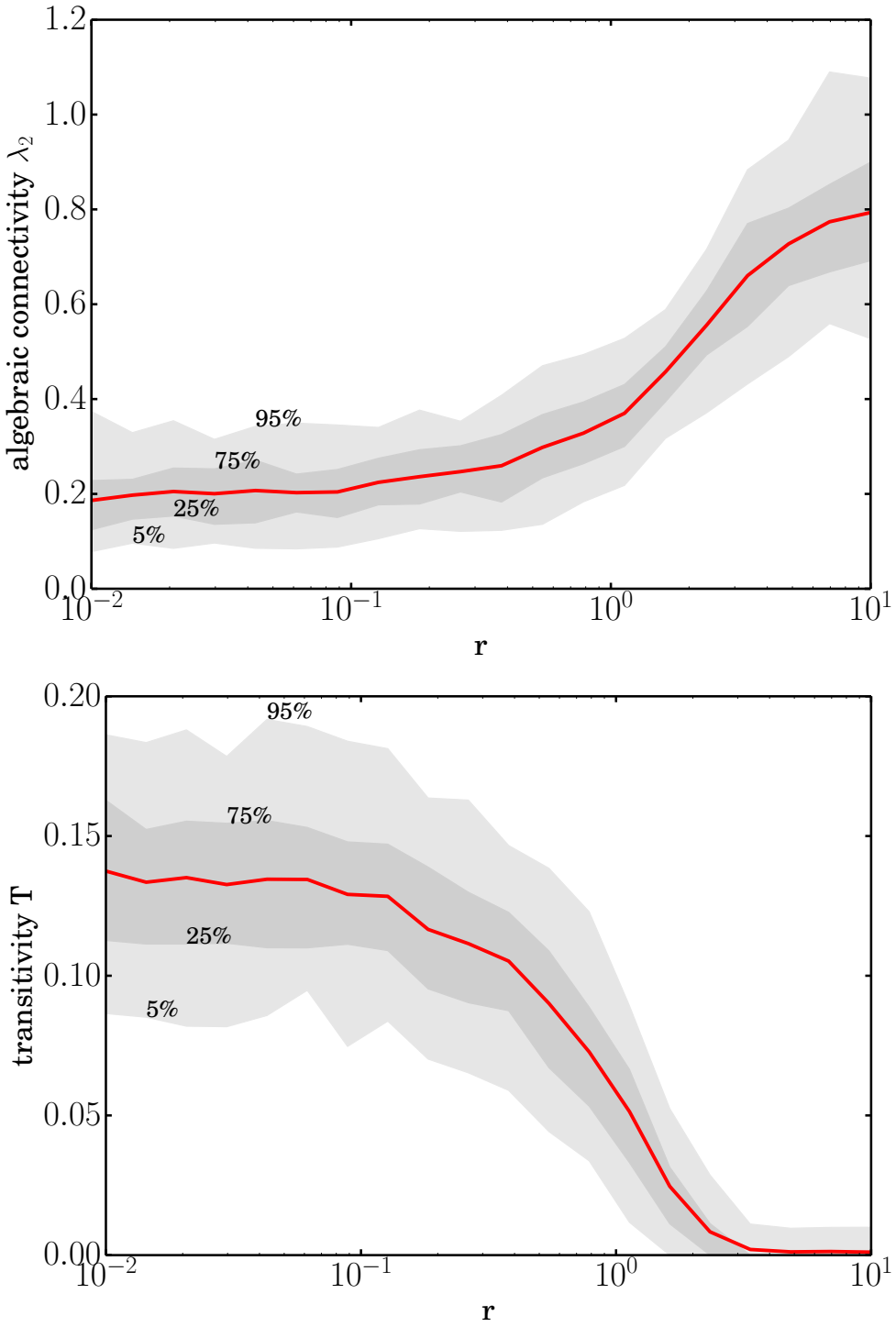

Fig. 5: Algebraic connectivity and transitivity of networks generated with the random power grid model. The parameters used are $\{N, N_0, p, q, s\} = \{100, 1, 0.3, 0.1, 0.2\}$. The solid red line gives the mean value and the shaded regions correspond to the 5-th, 25-th, 75-th and 95-th percentiles of the distribution for each r-value.

4 Trade-off with frequency stability: global redundancy

4.1 Single-node basin stability estimation

In the following, we give a brief description of single-node basin stability and the frequency stability estimation procedure that we apply. Each generator in the network, be it a net producer or net consumer, is modelled using the *swing equation* [10, 20]. This model is a good approximation for the short-term post-fault behaviour of a generator, i.e. the so-called first swing:

$$M\ddot{\phi}_i = P_i - \alpha\dot{\phi}_i - \sum_{j=1}^{N} a_{ij}\frac{|V_i||V_j|}{x_{ij}}\sin\left(\phi_i - \phi_j\right) , \tag{15}$$

where the dissipation α and the inertia M are constants that we assume to be equal for all nodes. We have chosen the line impedances x_{ij} to be proportional to the spatial distance of nodes i and j such that the mean value corresponds to a 200 km transmission line.

This system has a stable operating state with fixed rotor angles $\phi^* := (\phi_1^*, \ldots, \phi_N^*)$ and vanishing frequency deviations at each generator, i.e. $\omega^* := (0, \ldots, 0)$. Furthermore, there are also stationary states that need to be avoided, corresponding to periodic frequency oscillations in the power grid. Note that the fixed point of the system also leads to Eqn. 9 respectively 10. More precisely, for each step in a cascade, the stationary power flows are calculated, giving rise to a quasistationary process that acts on a much slower timescale than the transient dynamics described by the swing equation.

To estimate the single-node basin stability S_n of the stable operating state for a given node n, we create our initial conditions ensemble of size Ω by taking ϕ^* and ω^* and replacing their n-th entries with uniformly distributed random perturbations from the intervals $[-\pi;\pi]$ respectively $[-100;100]$. This corresponds to a disturbance of the stationary operating state at a single generator in the power grid. Then, S_n can be estimated as the number s of sampled initial conditions from which the system asymptotically converged to the fixed point, i.e.

$$S_n = \frac{s}{\Omega} . \tag{16}$$

At each sampled initial condition, the system either converges to the fixed point or not, hence we can regard the sampling as a sequence of independent identically distributed Bernoulli trials with a standard error of the mean given by

$$SEM = \sqrt{\frac{S_n\left(1 - S_n\right)}{\Omega}} . \tag{17}$$

As reported in [22,30], the single-node basin stability distribution shows three distinct groups of nodes with critical, fair and high stability. Due to the relatively small ensemble sizes we focus our analysis on the number of *critical* nodes with low $S_n < 1/3$ which allows a more reliable analysis instead of using the average single-node basin stability.

4.2 Results from Monte-Carlo simulations

For each value of the redundancy parameter r, we use an ensemble of 100 network realisations (cf. Sec. 3.3) with $N = 100$ nodes and the set of parameters

$\{N_0, p, q, s\} = \{1, 0.3, 0.1, 0.2\}$. For each network, we estimated the single-node basin stability distribution and from that the fraction of *uncritical* nodes N_u using an initial conditions ensemble of size $\Omega = 10$. N_u is the number of nodes n for which $S_n \geq 1/3$, i.e., all nodes with fair or high single-node basin stability.

Note that this choice of Ω leads to a comparatively large standard error of 16% in the worst case. However, it turned out that this choice results in a better trade-off (Sec. 4.3) than a larger number of trials but smaller number of networks, given constraints on the total computation time.

The dependence on r is shown in Fig. 6. Regarding the expected value of N_u, averaged over 100 network realisations at each value of r, we observe an increase from about 0.8 at $r = 0.01$ to about 0.95 at $r = 10$. Looking at the percentiles, we further observe that the distribution becomes very narrow for large values of the redundancy parameter, especially $r > 1$. This effect coincides with a strong increase of the algebraic connectivity (cf. Fig. 5). Hence, this increase of global redundancy drastically reduces the number of critical nodes $N_{crit} = N - N_u$ by more than 50% when r is increased in the considered parameter range. Further, 5% of the networks have up to 80% critical nodes for $r \ll 1$ while this low percentile of the network ensemble has only about 20% of critical nodes for $r \gg 1$.

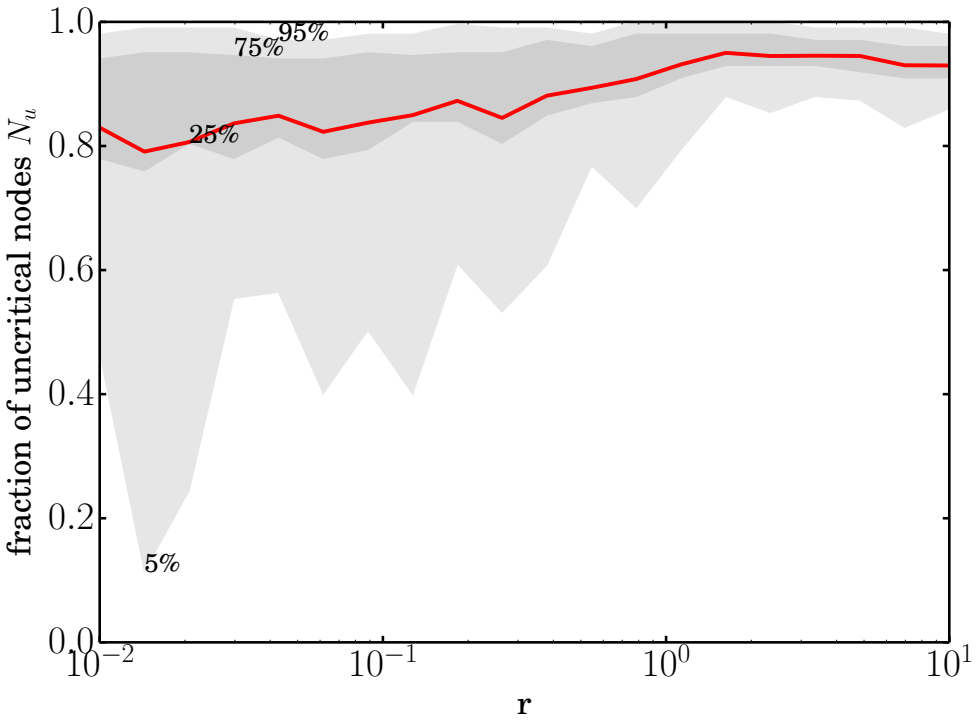

Fig. 6: Fraction of nodes with high or fair single node basin stability. The varied parameter r is the tuning parameter in the cost/redundancy optimisation function (Eqn. 13). The solid red line gives the mean value and the shaded regions correspond to the 5-th, 25-th, 75-th and 95-th percentiles of the distribution for each r-value. A linear regression of the mean gives a positive slope of 0.053 (p-value = $1.7 \cdot 10^{-9}$).

4.3 Trade-off

The parameter r (Eqn. 13) of the random power grid model [29] allows to tune between network topologies with local redundancy (high transitivity) and network topologies with global redundancy (high algebraic connectivity) without changing the average link density. Our simulations revealed that local redundancy reduces the vulnerability against cascading failures, whereas global redundancy reduces the number of critical nodes (poor single-node basin stability). These results are summarised in the overview Fig. 7. If the number of links or the total line length is limited, this poses a trade-off problem which is visualised in Fig. 8.

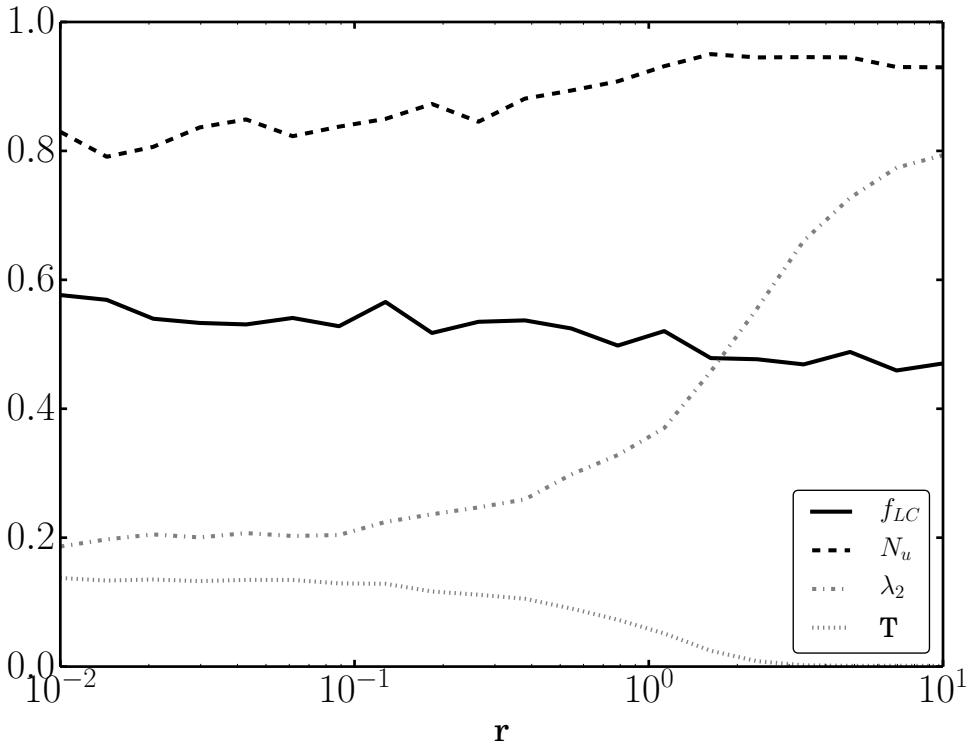

Fig. 7: Overview. Shown are the mean values of largest component remaining after cascading failure f_{LC}, the fraction of uncritical nodes N_u, the algebraic connectivity λ_2 and the transitivity T. The varied parameter r is the tuning parameter in the cost/redundancy optimisation function (Eqn. 13).

5 Conclusion

When studying the emergence of large-scale blackouts in power grids, frequency stability and resilience against cascading failures cannot be treated independently from each other. Frequency deviations may induce failures of single lines, leading to large-scale cascades of line trippings. At the same time, disconnection of generators or

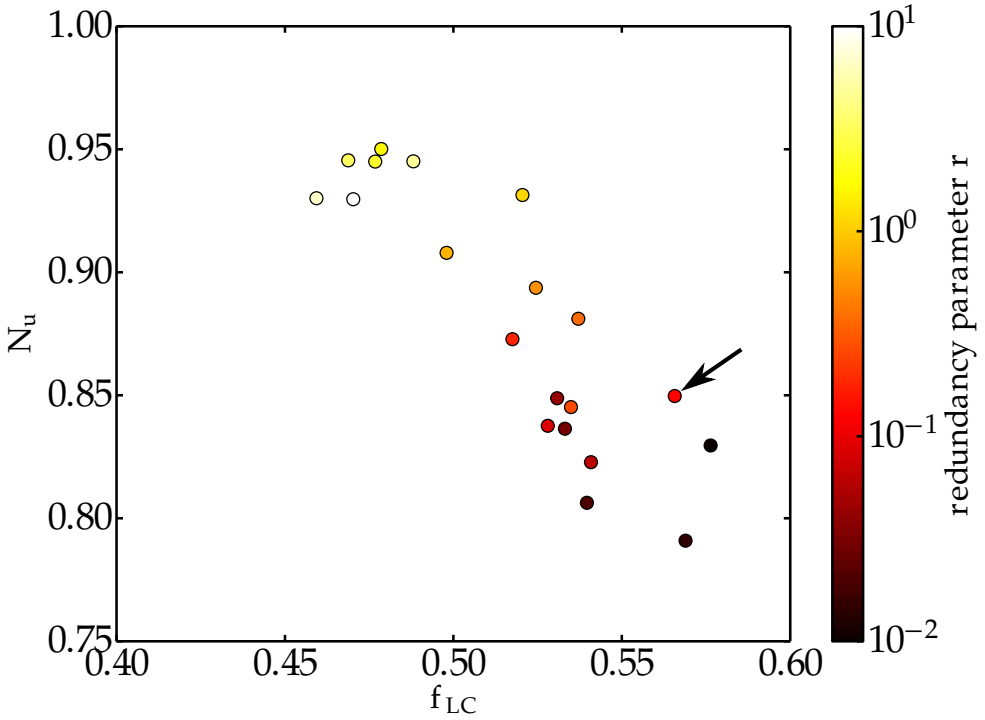

Fig. 8: Trade-off between average fraction of nodes with high and fair single node basin stability and the final largest component size after cascading failure. The arrow points to the recommended value of $r = 1/3$.

consumers causes power imbalances leading to frequency drops. For the stable operation of a grid it is therefore important to minimise the risk of frequency instabilities as well as cascading failures simultaneously. This fact has to be considered when building or extending power grids, since the topology of the grid has an important influence on the frequency stability and resilience against line failures.

We have found that the redundancy of lines is an important topological property in this context. Certainly, such redundancy of lines can be achieved in two different ways, either by adding long-range connections between distant nodes (global redundancy) or by connecting nodes which are close to each other (local redundancy). We have motivated that the global redundancy can be measured in terms of the algebraic connectivity but the local redundancy by the transitivity (Fig. 5).

It was shown that large transitivity leads to higher resilience against cascading failures (Fig. 4) whereas the number of critical nodes with poor frequency stability can be reduced by enhancing the global redundancy of the grid (Fig. 6). Since the total line length in a power grid is usually limited, mostly due to cost reasons and the spatial embedding, this leads to a trade-off problem (Fig. 8) which has to be addressed by finding an ideal balance between local and global redundancy in order to maximise the resilience against cascading failures as well as the frequency stability of the grid simultaneously.

Based on our insights, we recommend a heuristic rule-of-thumb for placing additional grid lines. One can choose a good r from the diagram (e.g. $r = 1/3$), and then add the additional line between those two nodes (or the new node and one of the old nodes) for which $f_r(i, j)$ is maximal. In other words, connect that pair of

nodes for which the quotient between the current network distance (plus one) and the cube of the spatial distance of the two nodes is maximal. Alternatively, one can calculate the algebraic connectivity and the transitivity for each possible placement of the additional line and choose the one where the improvement seems to be the best compromise.

Certainly, a more precise quantification of the trade-off is needed when these results should be applied to real power grids. Due to the computational effort of a single-node basin stability estimation, the simulations were done for networks of 100 nodes and relatively small ensemble sizes. In order to reduce the computational burden for simulations, further investigations should study the possibility of using fast, purely topology-based statistical estimators of basin stability [30] in this context. Further investigations could study the dependence of single-node basin stability estimators on r and use these instead of performing costly time-domain simulations. Furthermore, the cascading failure model could be improved by using a different excess capacity a for each node or by further investigating the parameter space of different uniform excess capacities. Also, a more detailed damage function for quantifying the damage of a cascading failure (e.g. size of lost demand or number of people affected) might be used.

The relationship between resilience against cascading failures and the existence of short detours around tripping lines should be investigated in more detail by including measures of higher-order transitivity that involve more than three nodes, i.e., detect short detours of length three or more [6].

Note that in this study we only considered transmission grids. It would also be interesting to apply the methods on distribution grids. These usually have a more tree-like topology, making them more vulnerable for cascading failures [3].

When the swing equation is extended by allowing variable voltages, also the voltage stability plays an important role in power grid dynamics [12,28]. This should be a next step for analysing cascading failures and comparing the different measures of power grid stability.

Since the increasing use of renewable energy resources requires structural changes and expansions of today's power grids it is important to develop strategies for connecting new generators and consumers to an existing grid without weakening its topology, especially since additional lines may actually worsen the situation in some cases [34]. However, we demonstrated that the usage of a single stability measure may not be sufficient to describe the dynamical complexity of a power grid. Hence, the comparison between cascading failure dynamics and basin stability is only a first attempt and we suggest to include other stability measures (e.g. survivability [15]) into the discussion as well.

We acknowledge gratefully the support of BMBF, CoNDyNet, FK. 03SF0472A (P.S., J.K.) and from the EIT Climate-KIC project SWIPO (J.H.).

References

1. 50hertz, `http://www.50hertz.com/Netzlast/Karte/index.html` (accessed: 08.06.2015)
2. S. V. Buldyrev et al. Nature, 464(7291), 1025-1028 (2010)
3. B. A. Carreras et al. Chaos 12.4 (2002): 985-994.
4. P. Crucitti, V. Latora, and M. Marchiori. Physical Review E 69.4 (2004): 045104.
5. T. Dewenter, and A. K. Hartmann. New Journal of Physics 17.1 (2015): 015005.
6. J. F. Donges. PhD Thesis. Humboldt University, Berlin, Germany, 2012.
7. F. Dörfler and F. Bullo. SIAM Journal on Control and Optimization 50.3 (2012): 1616-1642.

8. S. C. Srivastava, A. Velayutham and A. S. Bakshi, http://www.cea.nic.in/reports/articles/god/grid_disturbance_report.pdf (accessed: 27.04.2015).
9. Union of the Electricity Industry - EURELECTRIC, http://www.eurelectric.org/media/38999/eu_islands_-_towards_a_sustainable_energy_future_-_eurelectric_report_final-2012-190-0001-01-e.pdf (accessed 10.06.2015).
10. G. Filatrella, A. H. Nielsen, and N. F. Pedersen, Eur. Phys. J. B 61, 485 (2008).
11. C. Folke. Global Environmental Change 16 (2006): 253-267.
12. A. Gajduk, M. Todorovski and L. Kocarev. The European Physical Journal Special Topics 223.12 (2014): 2387-2409.
13. J. Gao et al. Physical Review Letters 107.19 (2011), 195701.
14. J. J. Grainger and W. D. Stevenson. Vol. 31. New York: McGraw-Hill, 1994.
15. F. Hellmann et al. arXiv preprint arXiv:1506.01257 (2015)
16. C. S. Holling. Annual review of ecology and systematics 4 (1973): 1-23.
17. P. Holme et al. Physical Review E 65.5 (2002): 056109.
18. Intergovernmental Panel on Climate Change, http://www.ipcc.ch/pdf/assessment-report/ar5/syr/SYR_AR5_FINAL_full.pdf (accessed: 27.04.2015).
19. J. C. Kile et al. Prehospital, Florian, and disaster medicine 20.02 (2005): 93-97.
20. J. Machowski, J. Bialek, and J. Bumby. John Wiley & Sons, 2011.
21. P. J. Menck et al. Nature Physics 9.2 (2013): 89-92.
22. P. J. Menck et al. Nature Communications 5 (2014): 3969.
23. A. E. Motter and Y.-C. Lai. Physical Review E 66.6 (2002): 065102.
24. D. E. Newman et al. IEEE Transactions on 60.1 (2011): 134-143.
25. T. Nishikawa and A. E. Motter, New J. Phys. 17, 15012 (2015).
26. Renewable Energy Policy Network for the 21st Century, http://www.ren21.net/Portals/0/documents/Resources/GSR/2014/GSR2014_full\%20report_low\%20res.pdf (accessed: 27.04.2015).
27. M. Rohden et al. Physical review letters 109.6 (2012): 064101.
28. K. Schmietendorf et al. The European Physical Journal Special Topics 223, 2577 (2014)
29. P. Schultz, J. Heitzig and J. Kurths. The European Physical Journal Special Topics 223.12 (2014): 2593-2610.
30. P. Schultz, J. Heitzig and J. Kurths. New Journal of Physics 16.12 (2014): 125001.
31. I. Simonsen et al. Physical review letters 100.21 (2008): 218701.
32. R. V. Solé et al. Physical Review E 77.2 (2008): 026102.
33. Union for the Co-ordination of Transmission of Electricity, http://www.entsoe.eu/fileadmin/user_upload/_library/publications/ce/otherreports/Final-Report-20070130.pdf (accessed: 27.04.2015).
34. D. Witthaut and M. Timme. New journal of physics 14.8 (2012): 083036.